Title
Cellular Features of the Mammalian Vestibular Epithelia Dependent Upon Head Movement-Driven Activity

Author
Prins, Terry John

Publication Date
2019

Peer reviewed|Thesis/dissertation

UNIVERSITY OF CALIFORNIA

Los Angeles

Cellular Features of the Mammalian Vestibular Epithelia Dependent Upon Head Movement-Driven Activity

A thesis submitted in partial satisfaction

of the requirements for the degree Master of Science

In Physiological Science

by

Terry John Prins

2019

ABSTRACT OF THE THESIS

Cellular Features of the Mammalian Vestibular Epithelia

Dependent Upon Head Movement-Driven Activity

by

Terry John Prins

Master of Science in Physiological Science

University of California, Los Angeles, 2019

Professor Larry F. Hoffman, Co-Chair

Professor Peter M. Narins, Co-Chair

The features of many peripheral sensory epithelia have been demonstrated to be labile to altered sensory inputs (Cummings et al., 1997; Mwachaka et al., 2015), however, the extent to which this is a global feature of the peripheral nervous system (PNS) has remained elusive. One way in which this can be studied is through investigations involving genetic mouse models for sensory hypofunction in the vestibular epithelia, since these peripheral structures are normally under constant sensory load throughout life. Here, it was investigated how altering vestibular sensory information to the inner ear epithelia (utricle, horizontal and superior cristae), using the otoferlin-null (*Otof-/-*) mouse may lead to presynaptic and/or postsynaptic changes in the expression of commonly expressed Ca^{2+} binding proteins oncomodulin (OCM, ß-parvalbumin) or calretinin (CALB2). No alterations were observed in the presynaptic expression of OCM or CALB2, however, there was a marked heterogeneous decrease in postsynaptic

CALB2 expression in the *Otof-/-* epithelia. These results suggest that some epithelial features (postsynaptic CALB2 expression) of the vestibular system are sensitive to the loss of OTOF and dynamic vestibular sensory inputs, while others (presynaptic OCM or CALB2 expression) are not. This may provide insight into how widespread the abilities of PNS sensory structures to adapt to changes in sensory information are, as well as how certain peripheral cellular features within the vestibular system are developed and maintained.

The thesis of Terry John Prins is approved.

Walter Helmut Metzner

Felix Erich Schweizer

Peter M. Narins, Committee Co-Chair

Larry F. Hoffman, Committee Co-Chair

University of California, Los Angeles

2019

TABLE OF CONTENTS

LIST OF TABLES AND FIGURES

ACKNOWLEDGMENTS

A very warm thank you to my friends and family, particularly my sister who has served as an exemplary role model for my entire life, as well as my committee members and mentor, Larry F. Hoffman, without whom this endeavor would not have been possible.

INTRODUCTION

Sensory adaptation in response to altered dynamic inputs has been studied for decades, in both central and peripheral nervous system structures. Most of this research is focused on the former, however, a few investigations have shed light on how peripheral structures may also be modified during periods of attenuated sensory input. For instance, monocular deprivation in rabbits has recently been shown to reduce the density of retinal ganglion cells in the visual system (Mwachaka et al., 2015), while removing auditory inputs to the cochlea will decrease the density of hair cell synapses (Liberman et al., 2015; Qi et al., 2019). For specific sensory systems, such as olfaction, synaptic recovery may even occur following a period of unilateral sensory deprivation (Cummings et al., 1997). These findings raise the question as to whether sensory epithelial changes are unique to individual systems, or whether they represent a more global ability of peripheral structures to adapt to alterations in the sensory environment.

One way in which global peripheral capabilities for sensory adaptation can be studied is via investigations with the vestibular epithelia, since vestibular inputs rely upon uniform Earth gravity that is static throughout an organism's life. Previous investigations have studied the effects of vestibular hypofunction (i.e. diminished vestibular input) by exposing mice or rats to microgravity environments (i.e. spaceflight), which results in modified synaptic densities within inner ear gravity receptors (Ross, 1994; Sultemeier et al., 2017). These results indicate that the vestibular epithelia are labile to sensory input, however, they do not explore how other common cellular features of the vestibular epithelia may be modified as a result of decreased input. Moreover, it is difficult to control for fluctuations in gravity that occur during takeoff and re-entry in these experiments, as well as the time delay between spacecraft landing and epithelial extraction. Earthbound genetic models provide greater control over vestibular hypofunction than spaceflight experiments, however, they have similarly not yet been used for studying how

hypofunction affects the development or maintenance of cellular features within the vestibular epithelia.

To help elucidate how distinct epithelial features may be altered due to vestibular hypofunction, the vestibular epithelia of three different mouse genotypes were compared: wild type (C57BL/6J; herein thereafter *WT*), otoferlin heterozygous (*Otof+/-*), and otoferlin-null (*Otof-/-*), the latter of which serves as a genetic model for vestibular hypofunction. This is because the otoferlin protein (OTOF) serves as a critical calcium sensor for neurotransmitter (NT) release in both cochlear and vestibular hair cells, which is compromised in *Otof-/-* animals (Roux et al., 2006; Beurg et al., 2008; Beurg et al., 2010). In vestibular epithelia, stimulus-evoked exocytosis (NT release due to head movement) has been shown to be compromised in calyx-associated (type I) hair cells of *Otof-/-* mice, while stimulus-evoked exocytosis in hair cells lacking a calyx (type II) is present with altered kinetics (Dulon et al., 2009). Interestingly, however, spontaneous exocytosis in type I hair cells of *Otof-/-* animals is likely preserved, since spontaneous excitatory postsynaptic currents have been reported in *Otof-/-* epithelia without stimulation (Dulon et al., 2009). These results make the *Otof-/-* animal a prime candidate as an earthbound model for vestibular hypofunction, since the loss of OTOF differentially effects the sensory input received by vestibular afferents from type I and type II hair cells, while concurrently preserving spontaneous inputs that occur independent of head movements.

While the findings of Dulon et al. (2009) indicate that the *Otof-/-* may be used as a model for vestibular hypofunction, they have thus far only been confirmed in a centralized region of the utricle known as the striola. Therefore, this study focused on how the loss of OTOF affects the expression of two commonly expressed centralized biomarkers in the utricle, horizontal and superior cristae: calretinin (CALB2) and oncomodulin/ß-parvalbumin (OCM). The primary advantage of studying the expression of these two proteins is that they both delineate centralized overlapping regions of the vestibular epithelia, except that CALB2 is expressed primarily in postsynaptic calyces and OCM in presynaptic hair cells (Desai et al., 2005b; Desai

et al., 2005a; Li et al., 2008; Hoffman et al., 2018). If either OCM+ hair cells or CALB2+ calyces are found to be altered within the epithelia of *Otof-/-* mice, it would indicate that the maintenance of these cellular features are likely dependent upon dynamic sensory inputs. Additionally, altered expression of OCM or CALB2 within *Otof-/-* vestibular epithelia would suggest that peripheral capabilities for sensory adaptation are more globally available than previously thought, and may provide critical insight into how epithelia may be targeted for sensory rehabilitation.

METHODS

Animals and Specimen Preparation

All procedures involving mice were approved by the UCLA Chancellor's Animal Research Committee (ARC), conformed to standards established in the *NIH Guide for the Care and Use of Laboratory Animals, Eighth Edition* (National Institutes of Health Publication, revised 2011), and adhere to the principles presented in the *Guidelines for the Use of Animals in Neuroscience Research* by the Society for Neuroscience (available from the Society for Neuroscience). Vestibular epithelia used for these experiments were obtained from three mouse genotypes: *WT*, *Otof+/-,* and *Otof-/-*. *Otof-/-* mice were obtained by crossbreeding an original cohort of genotyped *Otof-/-* animals, which were provided to our lab as a kind gift from Dr. Elisabeth Glowatzki (Johns Hopkins University), while *Otof+/-* mice were obtained by crossbreeding *WT* and *Otof-/-* individuals. All epithelia utilized and processed here were from adult mice (aged 80-125 days), which is after these epithelia are considered to be adult-like but well before epithelial expression of OCM and CALB2 are known to be reduced (Dechesne et al., 1994; Kevetter and Leonard, 2002; Simmons et al., 2010).

Prior to specimen dissection and within 24 hours of immunohistochemical processing, auditory brainstem responses (ABRs) were recorded from each mouse to confirm their genotype as *WT*, *Otof+/-*, or *Otof-/-*. Since OTOF is critical for exocytosis in cochlear inner hair cells, *Otof-/-* individuals show no ABRs in response to click stimuli for hearing thresholds between 30-80 dB SPL, while animals with one functional copy of the OTOF gene (i.e. *Otof+/-*) show ABRs comparable to the *WT* (Roux et al., 2006). Animals that did not show ABRs within this threshold range were thus confirmed as *Otof-/-*, while those that showed ABRs similar to the *WT* were confirmed as *Otof+/-*. While the genotypes of all animals used in this study were confirmed via ABRs, a few select epithelia from each genotype were also immunostained with anti-otoferlin (Abcam ab53233; anti-OTOF) to confirm the presence or absence of the OTOF protein in the *WT*/*Otof+/-* or *Otof-/-* animals, respectively.

After confirming the animal genotypes, vestibular epithelia were then extracted from the mice and fixed in preparation for immunohistochemical processing. Mice were deeply anesthetized with isoflurane and rapidly decapitated, after which fixative (4% paraformaldehyde in 0.1 M phosphate buffer) was immediately infused into the vestibule. Fixative was further flushed into the epithelia after opening the membranous labyrinth and applying a gentle stream of fixative solution. The temporal bones were then extracted and immersion-fixed on a rotating platform for 2 hours, followed by a wash with copious amounts of 0.1 M phosphate buffer saline (PBS). Three of the epithelia (utricle, horizontal and superior cristae) were microdissected and placed into a single well of a 96-well cell culture plate, while two (posterior crista and saccule) were placed into a separate well to serve as negative controls.

Thermolysin, Antibodies, and Immunohistochemistry

Previous investigations involving vestibular epithelia whole mounts have utilized a heat activated protease, known as thermolysin, to promote reagent penetration and to aid in specimen mounting (Desai et al., 2005b). Using a similar (albeit modified) protocol, all specimens shown here were first exposed to a thermolysin solution (1 µg thermolysin, 2 mM Tris 1 mM CaCl2) for 2.5-hours at 55ºC, followed by five washes of PBS spaced out by 10-minute rest intervals. Following the thermolysin treatment, each specimen was immersed in blocking solution (1% bovine serum albumin, 1% Triton X-100 in 0.1 M PBS) for 2 hours on a rotating platform. The blocking solution was then exchanged with a primary antibody cocktail, in which the specimens remained for 72 hours at 4ºC. Details about each of the individual primary antibodies (as well as the secondary antibodies) used within this study can be found in *Table 1*, which lists the target of the antibody, host in which it was raised, immunogen, manufacturer, and controls which verify the antibody's efficacy.

Most of the specimens reported here were exposed to a primary antibody cocktail containing a 1:250 working concentration of each of the following in blocking solution: anti-OCM

(labels OCM-positive hair cells), anti-CALB2 (labels CALB2-positive afferents and type II hair cells), and anti-ß-III-tubulin (anti-TUBB3, labels all afferents) (see *Table 1*). These antibodies allowed for the identification and quantification of OCM+ hair cells, CALB2+ hair cells, CALB2+ calyx distributions, total hair cells, and the differentiation between distinct hair cell phenotypes (i.e. type Is vs. type IIs) (Desai et al., 2005a). Primary antibody incubation was followed by a 3x wash with 0.1 M PBS for 10 minutes each (to ensure thorough removal of the primaries), after which each specimen was immersed in a secondary antibody solution.

Secondary solutions contained a 1:250 working concentration of Alexa 488 donkey anti-mouse, Alexa 555 donkey anti-goat, and Alexa 647 donkey anti-rabbit immersed in 0.1 M PBS (see *Table 1*). A 1:40 working concentration of fluorophore-conjugated Phalloidin (Biotium CF405M) was also added to the solution at this step to help identify the presence of all hair cells, using the kinocilium void as a guide during post-processing analyses (Li et al., 2008). Incubation in this secondary antibody solution lasted for 2 hours at room temperature, after which specimens were once again washed 3x with 0.1 M PBS (10-minutes each) before being whole mounted on glass slides filled with aqueous mounting media (Biotium 23001). Silicone spacers (Invitrogen S24737) were used to minimize the risk of tissue distortion caused by the placement of coverslips over the specimens, after which the samples were ready for confocal imaging.

Confocal Imaging and Analysis

All images reported here were obtained via confocal microscopy using a Zeiss LSM 710 confocal microscope (Oberkochen, Germany). Low-power image stacks were obtained using a Zeiss Neofluar 20x (0.8 NA) objective and provided an overview of the epithelia, while high-power image stacks were obtained using a Zeiss Apochromat 63x (1.4 NA) oil-immersion objective and used for collecting all immunofluorescence image data. It was apparent from the first few images that the distribution of CALB2+ calyces, but not OCM+ hair cells, was likely

altered in the *Otof-/-* animals. Therefore, the boundaries of the striola (or central zone) as defined by the presence of CALB2+ calyces could not be reliably determined in *Otof-/-* epithelia for high-power imaging (Desai et al., 2005a). Instead, high-power confocal stacks were imaged to cover an overlapping, juxtaposed region to the striola or central zone that harbors OCM+ hair cells (Hoffman et al., 2018), i.e. the *juxtastriola* (jStr; utricles) or *juxtacentral zone* (jCZ; cristae). For utricles, the jStr was imaged in four to five image stacks using 12-bit image depth intensity scaling, while four image stacks were sufficient to image the entire cristae (the jCZ as well as the planum). Following image acquisition, all high-power confocal stacks were then imported into *ImageJ* (*FIJI*) for measuring OCM and CALB2 hair cell fluorescence intensities or *Neurolucida* (MBF Bioscience Inc, Williston, Vermont, USA) for determining the density of CALB2+ calyces in the jStr or jCZ.

Since the level of hair cell OCM expression is variable between specimens, OCM+ hair cell counts were obtained by comparing jStr or jCZ hair cell fluorescence intensities to known OCM- hair cells from the periphery (i.e. extrastriola or planar regions). Circular contours (radius = 1.5 μm) were placed over each hair cell (at a depth where it was the widest) and measurement taken using the *measure* command, which generates a value representing the average fluorescence intensity per pixel within the contour. Intensity measurements were obtained for hair cells both within the jStr/jCZ, as well as fifty measurements outside of this region (background intensities) which were used to establish an intensity threshold. If a hair cell within the jStr/jCZ region exhibited a fluorescence intensity value equal or greater than 4 standard deviations (∂_{bf}) above the average (I_{bf}) background intensity ($I_{bf} + 4 \bullet \partial_{bf}$), then there was an extremely low probability ($p < 0.0001$) that the hair cell was negative for OCM expression (Hoffman et al., 2018). This approach provided an objective measure for which OCM+ hair cells could be determined, while reducing the likelihood of generating false positive or negative OCM hair cell counts that come with using more subjective measures (i.e. visually). A similar approach was utilized for CALB2+ type II hair cell counts in the medial extrastriola (a

135x135 μm region medial to the jStr), except that threshold intensities were obtained from known CALB2- type I hair cells within this region as delineated by TUBB3.

After the OCM and CALB2 hair cell quantification was complete, image stacks were then imported into *Neurolucida* and stitched together for CALB2+ calyx quantification within the jStr or jCZ. Immunolabeling involving CALB2+ calyces was particularly robust and did not express the same heterogenous level of expression as OCM within the jStr. Therefore, distributions of CALB2+ calyces were determined without establishing intensity thresholds (i.e., the method used for hair cell OCM or CALB2) and were quantified visually for the jStr and jCZ. Total hair cell counts, as well as the identification of hair cell phenotypes (i.e. type I and type II), were also determined here by identifying the presence of a kinocilium void (using fluorophore conjugated Phalloidin) and the presence or absence of a TUBB3+ calyx, respectively. These counts were used for the postsynaptic CALB2 analyses presented in *Figures 3* and *4*.

Statistics (Bootstrap Resampling)

For all of the analyses represented herein, a bootstrap resampling strategy was employed to test several null hypotheses regarding the distributions of various hair cell or calyx phenotypes within the jStr or the jCZ. The null hypotheses in question were that the normalized empirical counts (n=3, each genotype) for specific hair cell (OCM+ or CALB2+) or calyceal (CALB2+) phenotypes were similar to those derived from random sampling from all of the data (*WT, Otof+/-,* and *Otof-/-*). For hair cells, the empirical data was first analyzed by a two-way ANOVA, whereby the *F*-statistics for each fixed effect of genotype (i.e. *WT*, *Otof+/-*, and *Otof-/-*), hair cell phenotype (e.g. OCM+/OCM-), and the interaction effect were produced and stored in *R*. All hair cell phenotypes were then stored in a virtual dataframe, which was resampled from using the total number of hair cells quantified from the empirical data (8347 measurements, OCM; 2862 measurements, CALB2). The resampled data was analyzed using the same two-way ANOVA described above, with the *F*-statistics for genotype, hair cell phenotype, and the

interaction effect stored. This process for the resampled data was repeated 10,000 times to create an *F*-statistic distribution for each effect, which was then used to test the null hypothesis by comparing the empirically derived *F*-statistics with those generated through random resampling. A similar procedure was employed for analyses involving CALB2+ calyx densities, except that a density value was generated and analyzed with the resampled data, and/or the list of fixed effects included epithelial region (i.e. rostral, middle, or caudal jStr). For both sets of analyses, if any of the empirically obtained *F*-statistics were found to be outside the resampled *F*-statistic distributions, then the probability of obtaining the observed hair cell (or calyx) phenotypes due to random associations between genotype was less than 0.0001.

RESULTS

OTOF immunolabeling and ABRs are absent in Otof-/- *animals*

It was first established that there was no OTOF immunolabeling throughout the epithelia of the *Otof-/-* animals and that these subjects exhibited no auditory responses to click sound stimuli of varying intensities. These results are illustrated in *Figure 1*, whereby hair cells throughout the WT utricle were positively labeled using a mouse anti-OTOF antibody (green; Abcam ab53233), which was not observed in the *Otof-/-* epithelia. Afferent calyces, which are positively identified via TUBB3 immunolabeling (grayscale) were found throughout the epithelia of all three genotypes. These data indicate that there is no OTOF protein found throughout the epithelium of *Otof-/-* mice and that the general architecture of the epithelium (i.e. the presence of afferent calyces) is preserved (*Figure 1A-B*) (Prins et al., 2019). The horizontal and superior cristae were processed in an identical fashion and yielded similar results (data not shown). No observable differences in OTOF or TUBB3 immunolabeling were observed between the *WT* and *Otof+/-* specimens. While only a few select epithelia were immunolabeled for the OTOF protein, all mice in the present study were subjected to an ABR protocol to confirm their genotypes prior to IHC processing. *Otof-/-* mice do not exhibit responses to click sound stimuli within normal hearing thresholds (30-80 dB SPL), while *Otof+/-* mice exhibit responses similar to the *WT* (Roux et al., 2006). A few responses from mice representative of each genotype are illustrated in *Figure 1C*, demonstrating that the genotypes of *Otof-/-* or *Otof+/-* mice used in this study can be readily confirmed via this method.

Total number of OCM+ hair cells is preserved in the vestibular epithelia of Otof-/- *mice*

Following genotype confirmation via ABRs, it was first investigated whether the loss of OTOF leads to a presynaptic change in OCM expression. From the onset of these experiments, it was apparent from low-power confocal micrographs that the overall distributions of OCM+ hair cells were preserved between the three mouse genotypes (*Figure 2A-C*). The total number of

OCM+ hair cells were quantified (see *Methods*) for 9 epithelia (3 each of utricle, horizontal and superior crista) for each genotype, the results for which are shown in *Figure 2D-F*. Using bootstrap resampling statistics, it was determined that the total number of OCM+ hair cells were similar across genotype, since the probability of obtaining the empirically observed number of *Otof-/-* OCM+ hair cells via random sampling across all genotypes and specimens was p=0.257 (*Figure 2G*). Therefore, it is likely that the distribution of OCM+ hair cells are unaltered in the *Otof-/-* animals, and the OCM+ region (jStr or jCZ, outlined by the cyan dashed line in *Figure 2*) could be used as a region of interest for subsequent analyses with CALB2 (as it was consistent between mouse genotypes).

Density of jStr and jCZ CALB2+ calyces is altered in the epithelia of Otof-/- *animals*

Since the loss of OTOF is known to cause decreased stimulus-evoked exocytosis in type I hair cells (Dulon et al., 2009), postsynaptic expression of CALB2+ in afferent calyces was also investigated in the epithelia of *Otof-/-* mice. As illustrated in *Figure 3*, low-power confocal micrographs of the utricular striola revealed that postsynaptic calyceal CALB2 expression (arrows) was reduced in the *Otof-/-* specimens. The horizontal and superior cristae yielded similar results, which appeared to have fewer CALB2+ calyces in each epithelium overall (*Figure 3B-C*). From these confocal micrographs, CALB2+ calyx fractions (relative to total striolar calyces) were quantified for the jStr (utricles) or jCZ (cristae), revealing that CALB2+ calyx fractions were attenuated in the epithelia of *Otof-/-* animals (*Figure 3D-F*). The null hypothesis (see *Methods*) was tested through a resampling protocol, whereby the probability of obtaining the empirically observed CALB2+ calyx fractions in the *Otof-/-* epithelia from randomly sampling across all genotypes was found to be less than 0.0001. These data indicate that, while presynaptic OCM hair cell expression is preserved in epithelia lacking the OTOF protein, postsynaptic expression of CALB2 is not.

The observed decrease in CALB2+ calyx densities was also found to be heterogeneous throughout the jStr of the *Otof-/-* utricles. *Figure 4* illustrates, through maximum intensity projections of high-power confocal micrographs, that the density of CALB2+ calyces were noticeably reduced in the middle or caudal regions of the *Otof-/-* jStr, while the rostral regions appeared comparable to the *WT* or *Otof+/-* epithelia. Via bootstrap resampling, the null hypothesis was tested that the density of CALB2+ calyces observed in the *Otof-/-* utricles could be obtained by random sampling calyx phenotypes (CALB2+ and CALB2-) from across all genotypes and jStr regions. It was found that there was an effect of genotype on CALB2+ calyx densities ($p<0.0001$), a regional effect ($p=0.009$), as well as a genotype/region interaction ($p=0.010$). Interestingly, no differences were observed between the *WT*, *Otof+/-*, and *Otof-/-* rostral regions of the jStr (Newman-Keuls, *WT*-*Otof-/-* $p=0.468$; *Otof+/--Otof-/-* $p=0.549$). These data indicate that the postsynaptic expression of CALB2 within the rostral jStr is unaffected by the absence of the OTOF protein, and that the degree of postsynaptic CALB2 expression loss in *Otof-/-* utricles is dependent upon jStr region.

Total number of CALB2+ type II hair cells are not diminished in the vestibular epithelia of Otof-/- *mice*

The hypothesis was also tested that the observed decrease in CALB2 expression was exclusively a postsynaptic phenomenon and was not also observed presynaptically in type II hair cells. If the expression of CALB2+ type II hair cells were different between the three mouse genotypes, then it would suggest that observed altered CALB2 expression postsynaptically may not due to the deletion of the OTOF gene, but rather, a disruption in global gene networks following the loss of OTOF. This was investigated by comparing the total number of CALB2+ type II hair cells in the medial extrastriola of the utricle from each genotype, using a resampling paradigm (*Figure 5*). High-power confocal micrographs did not yield a noticeable difference in the number of CALB2+ type II hair cells in the utricular medial extrastriola (*Figure 5A-C*), which

was confirmed via resampling strategy similar to that performed for OCM (p=0.589; *Figure 5D*). Therefore, the number of extrastriolar CALB2+ type II hair cells in the *Otof-/-* utricles are similar to their *WT* and *Otof+/-* counterparts, and the loss of OTOF does not lead to a wholesale disruption of utricular CALB2 expression.

DISCUSSION

Some presynaptic cellular features are preserved in vestibular epithelia following the loss of OTOF

It was investigated in the present study how certain cellular features of the vestibular epithelia may be modified in the *Otof-/-* mouse, which is an earthbound genetic model for vestibular hypofunction. Within the striolae of *Otof-/-* utricles, stimulus-evoked exocytosis is severely compromised (type I hair cells) or otherwise altered (type IIs) that leads to an attenuation of vestibular sensory inputs to these epithelial regions (Dulon et al., 2009). This decreased vestibular input may, thus, result in either presynaptic alterations to certain cellular features, postsynaptic alterations, or some mixture of the two. Presynaptically, it has been shown that the loss of OTOF does not affect the overall level of OCM expression in either type I or type II hair cells (Prins et al., 2019), however, may still have had an effect on the total number of OCM+ hair cells within the jStr or jCZ epithelial regions. Here, it has been demonstrated through a rigorous bootstrap resampling paradigm that this was not the case (*Figure 2*), and that the total number of OCM+ hair cells is preserved even in the event of congenital vestibular hypofunction. This was true for each vestibular epithelium investigated (utricle, superior, and horizontal cristae), and suggests that at least presynaptically, some features of the vestibular epithelia are preserved in the absence of OTOF and dynamic sensory inputs.

Postsynaptic alterations in CALB2 and the effect of losing OTOF in vestibular epithelia

While the total number of OCM+ hair cells was conserved presynaptically between the three genotypes, it was apparent from the start of this investigation that there was a pronounced decrease in the total number of postsynaptic CALB2+ calyces in *Otof-/-* epithelia. Bootstrap resampling statistics (*Figure 3*) confirmed that there was a very low probability ($p<0.0001$) of obtaining the CALB2+ calyx densities observed in the *Otof-/-* epithelia via random sampling across all genotypes, demonstrating a clear postsynaptic change in *Otof-/-* epithelia following

the loss of OTOF. Additionally, this postsynaptic decrease in CALB2 expression was reported in reference to all calyces (i.e. as a calyx fraction or density) and is not due to calyceal retraction, which has not been observed in *Otof-/-* epithelia (Prins et al., 2019). Decreased CALB2+ calyx densities were also not exclusive to the utricular jStr, as the observed calyceal CALB2 decreases were also present in the jCZ of the horizontal and superior cristae. These findings strongly suggest that the postsynaptic expression of CALB2 is dependent (in part) upon the presence of the OTOF protein, and that this OTOF dependence is not exclusive to the utricle.

So why then, does the loss of the OTOF protein result in changes to postsynaptic CALB2 and not presynaptic CALB2 or OCM? The findings of Dulon et al. (2009) strongly suggest that the loss of OTOF results in a disconnect between hair cell stereocilia deflection and the amount of neurotransmitter quanta released onto afferent calyces. Therefore, sensory inputs to vestibular afferents as a result of head movement are reduced or otherwise severely compromised, whereas stereocilia deflections at the level of the hair cell would remain intact (Dulon et al., 2009). This would likely lead to a differential influx of pre- and postsynaptic Ca^{2+}, which may reduce the need for calyces to buffer intracellular Ca^{2+}, but not for vestibular hair cells. Additionally, studies from other systems have shown that both OCM and CALB2 are likely playing a role in regulating intracellular Ca^{2+} (Schiffmann et al., 1999; Hackney et al., 2005; Tong et al., 2016), and that hair cells receive Ca^{2+} influx through voltage-gated Ca^{2+} channels (Su et al., 1995; Martini et al., 2000; Dulon et al., 2009; Vincent et al., 2014) and calyces through GluR2 containing AMPA receptors (Dememes et al., 1995; Bonsacquet et al., 2006). Given these observations, a decreased need to buffer intracellular Ca^{2+} postsynaptically may lead to decreased CALB2 expression, and may be responsible for the observed *Otof-/-* epithelial changes reported here (*Figure 3*) (Dulon et al., 2009). This interpretation is further reinforced by the results from *Figure 5*, whereby CALB2 expression in utricular hair cells was found similar between the three genotypes.

Interestingly, the decrease in CALB2+ calyces observed in the *Otof-/-* epithelia was also not found to be homogeneous throughout the utricular jStr. For instance, it was reported here that there was no discernable difference in the densities of CALB2+ calyces between the rostral jStr of the three genotypes, however, there was a marked decrease in the middle and caudal regions (*Figure 4*). The horizontal and superior cristae were also analyzed for rostral-caudal differences in CALB2 expression, but were found to be similar between the three genotypes (two-way ANOVA, $p>0.05$). One possible explanation for the utricular change is that stimulus-evoked exocytosis in type I hair cells is less dependent upon the OTOF protein within the rostral striola compared to the other centralized regions of the utricle. However, there is substantial evidence that hair cell OTOF interacts with SNARE proteins in a similar manner to synaptotagmin (Ramakrishnan et al., 2014), and thus far synaptotagmin isoforms have not been found presynaptically (Safieddine and Wenthold, 1999; Sudhof, 2004). Thus, this explanation is unlikely, since it is much more likely that the rostral jStr region is also OTOF dependent and that the OTOF protein is required for normal vestibular function throughout the epithelium.

There are two other, more possible explanations as to why the expression of CALB2 in calyces of the rostral jStr were found to be similar between the three mouse genotypes. The first involves the way both CALB2 and AMPA receptor subunits are expressed in mice as animals age: calyx CALB2 expression is first detected at embryonic day (E) 18 and peaks by postnatal day (P) 14 (Dechesne et al., 1994), while GluR2 is detected at E12 and continues throughout synaptogenesis (Puyal et al., 2002). Since it has been shown that inner hair cells are not dependent upon OTOF for stimulus-evoked exocytosis until P14 (Beurg et al., 2010), it is possible that the rostral jStr begins to express CALB2 before the middle and caudal regions when hair cells are still OTOF independent. However, this explanation would necessitate vestibular hair cells also exhibit OTOF independence until P14 like the cochlea, as well as CALB2 expression appearing first in the rostral striola, both of which have not yet been shown. The second interpretation involves the way rostral jStr calyces receive inputs from efferent

neurons as well as afferent-contiguous type II hair cells. Efferent neurons can provide feedback to the rostral utricle from the semicircular canals during regular head tilts associated with locomotion (Plotnik et al., 2002), while type II hair cells can provide direct inputs to calyces through “outer face” synapses (Moser et al., 2006). These inputs, while attenuated in the *Otof-/-* animals, may be sufficient to preserve the CALB2+ calyces within the rostral jStr, as locomotion would result in more pronounced efferent input into this region.

Conclusion

In summary, we sought to investigate how certain cellular features of the vestibular epithelia of mice may be dependent upon dynamic vestibular inputs, using the *Otof-/-* mouse as a model for vestibular hypofunction. While it has been previously shown that the overall topography and architecture of the vestibular epithelia are preserved in *Otof-/-* animals (Prins et al., 2019), it was unclear whether other pre- or postsynaptic features of the vestibular epithelia may be affected by the loss of OTOF, and more importantly, the loss of dynamic vestibular inputs. The results presented here demonstrate that there are clear postsynaptic changes (i.e. calyx CALB2 expression) that result from the loss of vestibular inputs, but that this loss is not uniformly represented within the epithelia of *Otof-/-* animals. Crucially, these data suggest that there are possibly specific interactions between the different epithelia (i.e. rostral jStr and cristae ampullares) that can modulate the expression of certain proteins (CALB2) through efferent feedback, or that the expression of postsynaptic CALB2 may be downregulated in response to reduced needs to buffer intracellular Ca^{2+}. Nevertheless, these data show that there are distinct epithelial features of the vestibular system that are labile to sensory inputs, and that more epithelial features of these peripheral structures are dependent upon sensory inputs than previously thought.

FIGURES

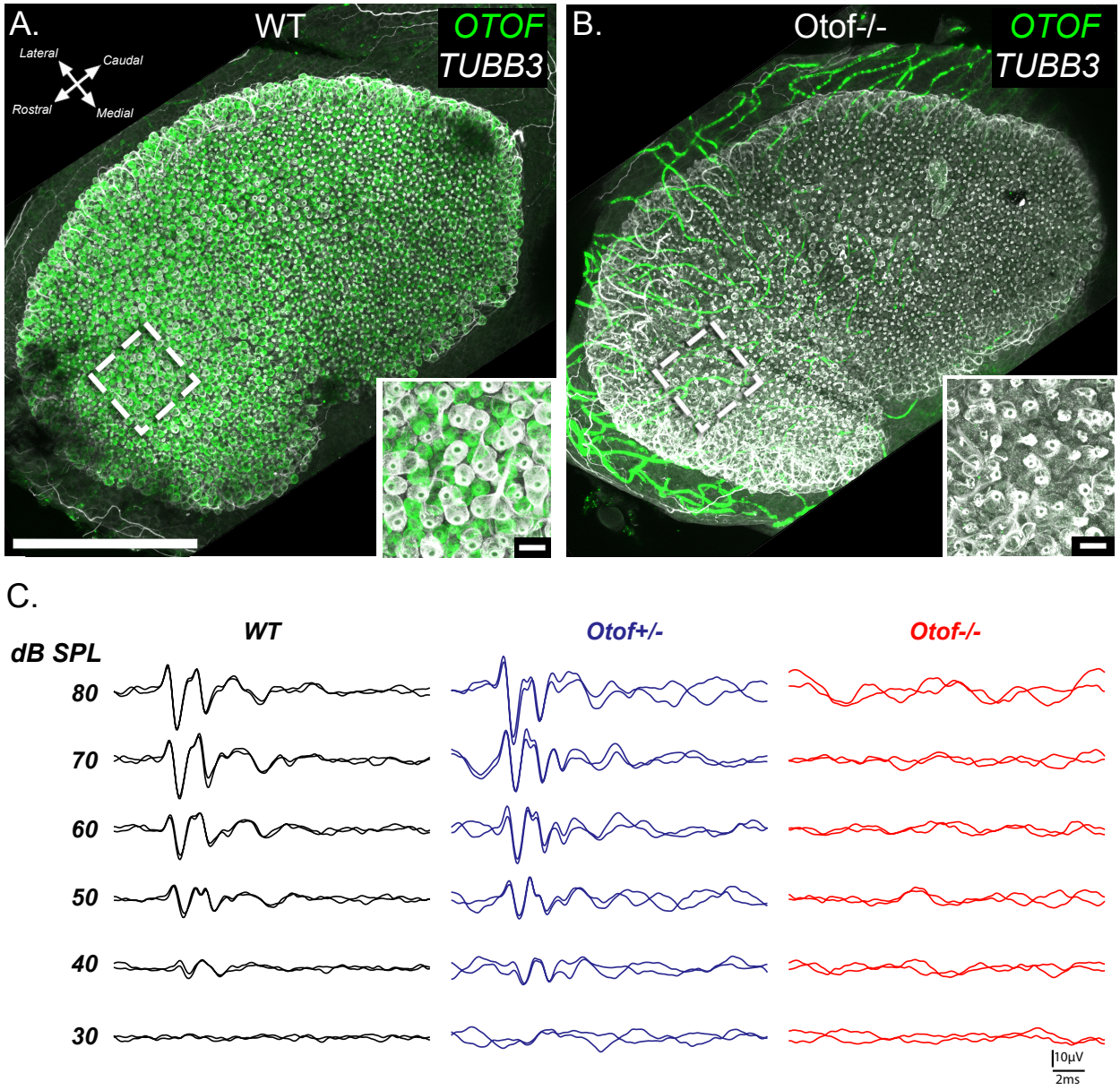

Fig. 1: OTOF immunolabeling and ABRs confirm the genotypes of Otof-/- *mice.* A-B. Low-power (20x) confocal micrograph maximum intensity projections of a *WT* (A) or *Otof-/-* (B) utricle confirming the presence (*WT*) or absence (*Otof-/-*) of the OTOF (green) protein, respectively (scale bars = 200 μm). Insets show higher resolution 63x maximum intensity projections from each specimen, obtained from the region indicated by the dashed white boxes, with TUBB3 (grayscale) present in the *Otof-/-* utricle but no observable OTOF (scale bars = 10 μm). C. Superimposed, replicable, ABRs recorded from each of the three genotypes (*WT,* black; *Otof+/-*

, blue; *Otof-/-*, red) in response to various click sound stimuli with intensities ranging from 30-80 dB SPL. Within these ranges, *Otof+/-* mice exhibit ABRs comparable to the *WT* while the *Otof-/-* animals do not.

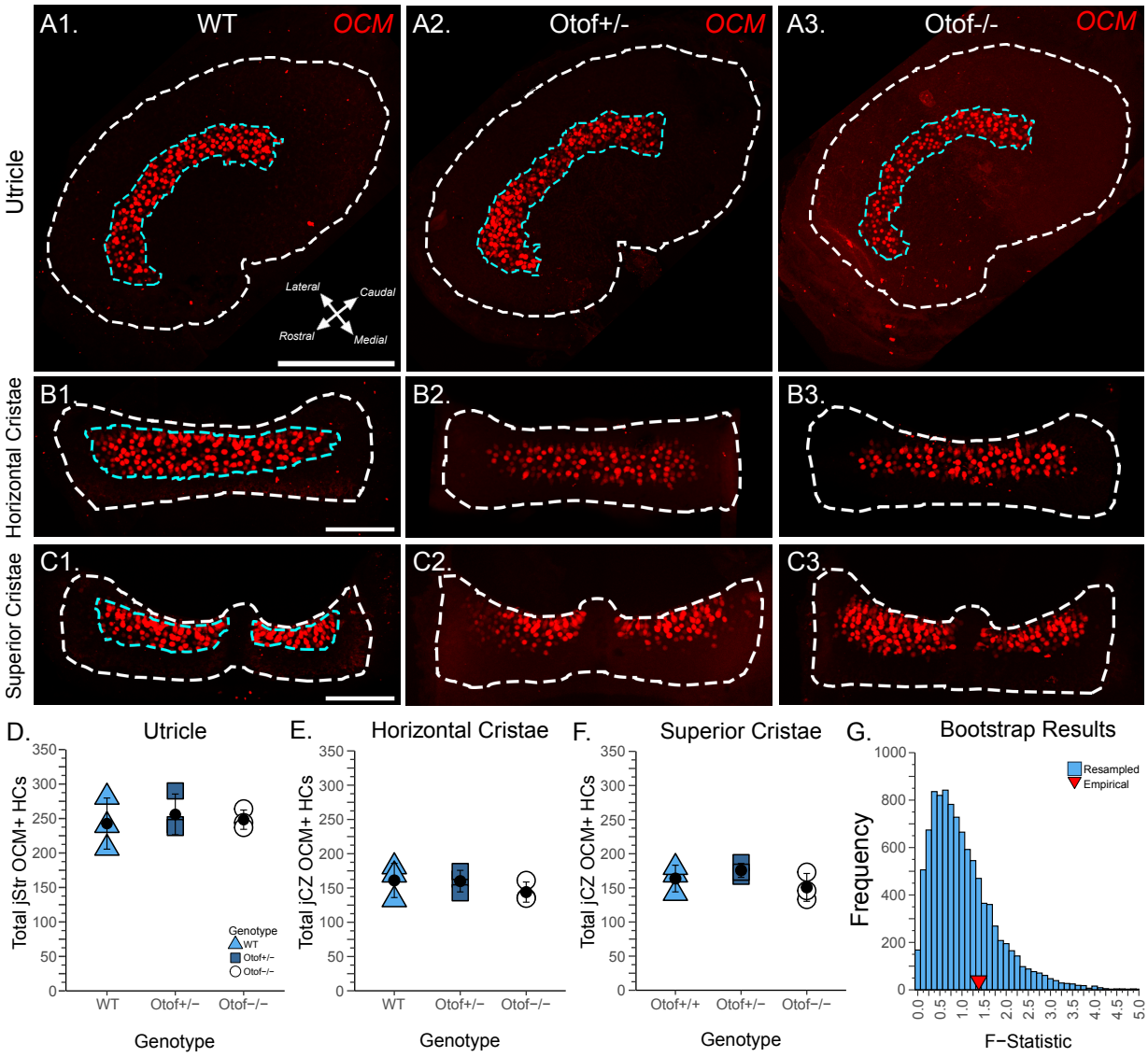

Fig. 2: Otof-/- *mice exhibit similar numbers of OCM+ hair cells in the utricle and horizontal cristae when compared to their* WT *and* Otof+/- *counterparts.* Maximum intensity projections generated from low-power (20x) confocal micrographs revealed similar distributions of OCM+ hair cells (red) in *WT* (A1-C1), *Otof+/-* (A2-C2), and *Otof-/-* (A3-C3) mice. A. The OCM+ hair cell regions were used to define the *juxtastriola* (jStr) for subsequent analyses (outlined by the cyan, dashed line), whose location is shown relative to the extent of the entire epithelium (white dashed line) in each of the three genotypes (scale bars = 200 μm). B-C. The OCM+ region in the horizontal (B) and superior (C) cristae was also comparable between the three genotypes, which was used to identify the *juxtacentral zone* (jCZ, cyan dashed line), highlighted here only in

the *WT* specimens (scale bars = 100 μm). D-F. Point plots showing the total counts of OCM+ hair cells in the utricles (D), horizontal cristae (E), or superior cristae (F) between the three genotypes, with *WT* numbers represented by triangles, *Otof*+/- by squares, and *Otof*-/- by open circles (closed circles = mean; error bars = 1 SD). G. Bootstrap resampling distribution showing computed two-way ANOVA *F*-Statistics (genotype) using resampled OCM+ hair cell counts from all three genotypes and epithelia (blue), with the empirical *F*-Statistic superimposed (inverted red triangle). The probability of obtaining this empirical *F*-Statistic from resampled data is p=0.257.

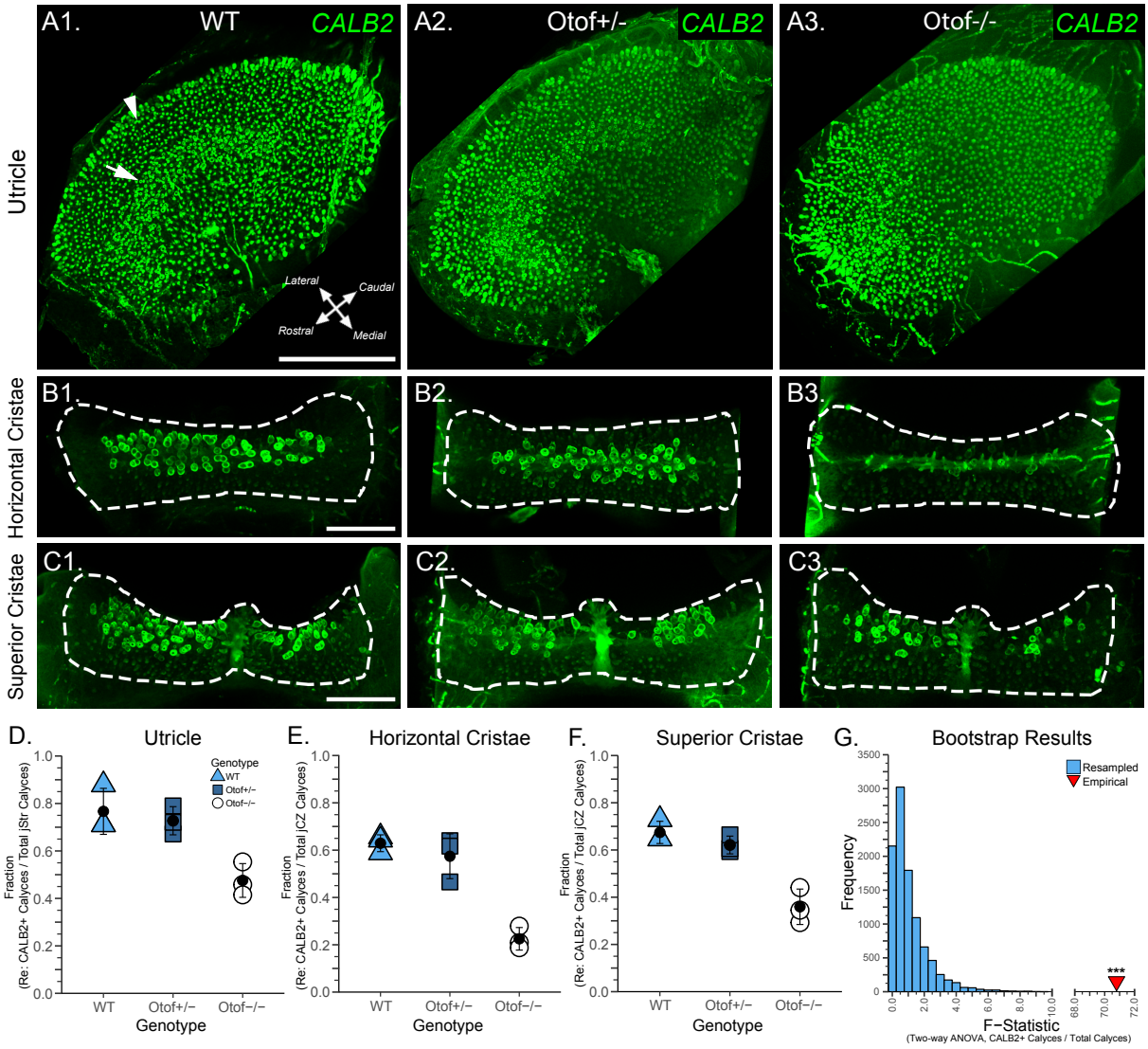

Fig. 3: Otof-/- *mouse epithelia exhibit fewer CALB2+ calyces than their* WT *or* Otof+/- *counterparts.* Maximum intensity projections generated from low-power confocal micrographs of mouse epithelia revealed a heterogeneous change in CALB2 expression (green) in calyceal afferents of *Otof-/-* mice (3) when compared to either the *WT* (1) or *Otof+/-* (2) epithelia. A. Utricle maximum intensity projections suggest conserved CALB2 expression in type II hair cells (arrowheads) of the three mouse genotypes, while there is a marked decrease of CALB2 expression in afferents (arrows) of the *Otof-/-* specimens (scale bar = 200 µm). B-C. Similar differences in CALB2 calyx expression were observed throughout the horizontal (B) and superior (C) cristae, with the extent of the entire epithelium shown by the white, dashed lines for

clarity (scale bars = 100 μm). E-F. Point plots showing the fraction of calyces found to express CALB2 among the different epithelia, with *WT* numbers represented by triangles, *Otof+/-* by squares, and *Otof-/-* by open circles (closed circles = mean; error bars = 1 SD). G. Bootstrap resampling paradigm by which the probability of obtaining the empirically observed (inverted red triangle) *F*-Statistic (two-way ANOVA, genotype) via random resampling was less than 0.0001.

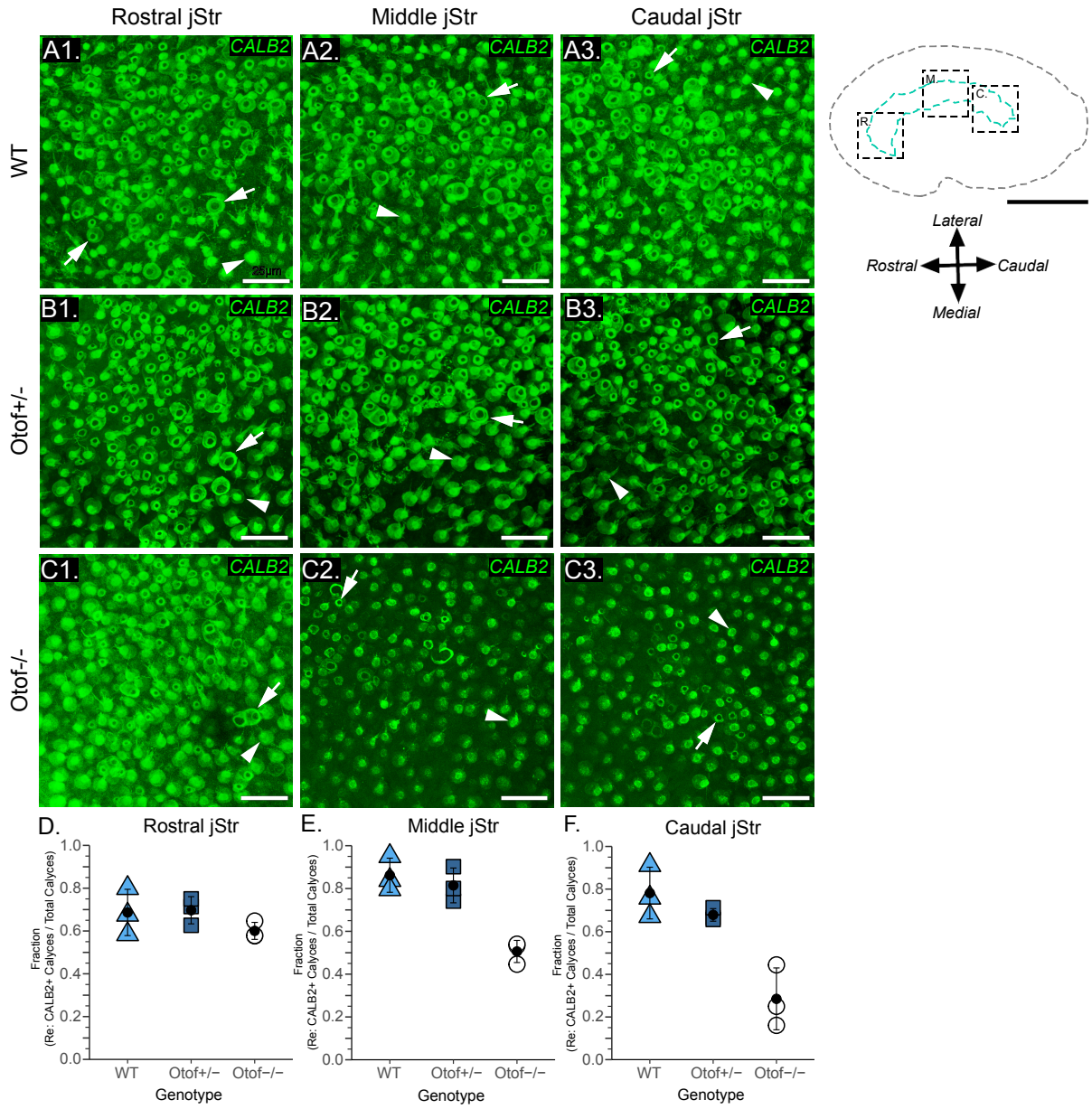

Fig. 4: Severity of CALB2+ calyx attenuation in the Otof-/- *mouse utricle is dependent upon jStr region.* A-C. Maximum intensity projections generated from high-power confocal micrographs showing CALB2+ afferent calyces (arrows) and CALB2+ type II hair cells (arrowheads) in *WT* (A1-3), *Otof+/-* (B1-3), and *Otof-/-* (C1-3) mice for each of the given jStr regions (rostral, middle, caudal; scale bars = 25 μm). D-F. Point plots demonstrating the fraction of jStr calyces expressing CALB2 in each of the utricular regions by genotype (*WT* = triangles, *Otof+/-* = squares, *Otof-/-* = open circles; closed circles = means; error bars = 1 SD). Bootstrap resampling statistics (see *Methods*) revealed that the probability of obtaining any of the

observed CALB2+ calyx fractions by randomly resampling across all three regions and genotypes is less than 0.0001. Resampling analyses also revealed a regional effect on CALB2+ calyx fractions ($p=0.009$) as well as a genotype/region interaction ($p=0.010$). A Newman-Keuls post-hoc analysis revealed a difference between the middle and caudal regions of the *Otof-/-* animals compared to the *WT* or *Otof+/-* ($p<0.01$), while rostral regions were similar to *WT* ($p=0.468$) and *Otof+/-* ($p=0.549$). On the right: Locations of the jStr (cyan dashed line) regions compared between the three genotypes in A-C (rostral, middle, and caudal), as shown by black dashed boxes in a template of the utricle (scale bar = 200 μm).

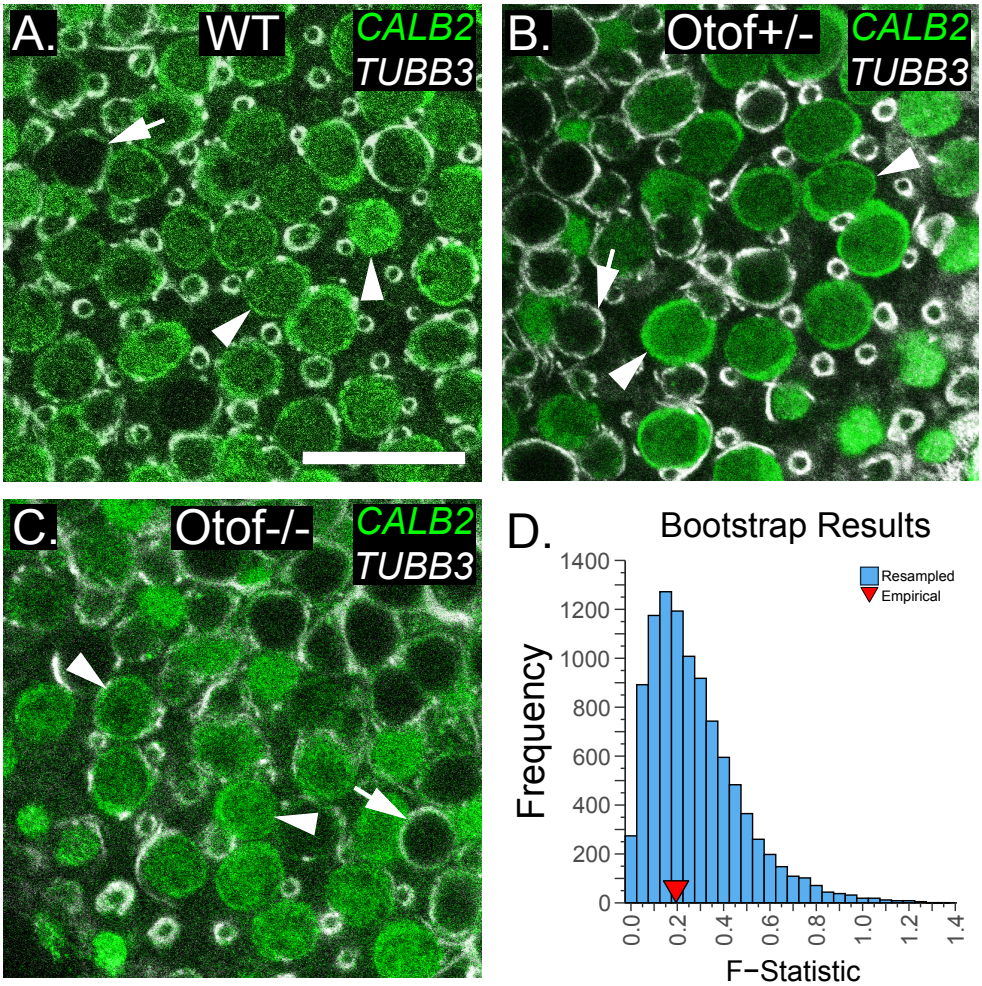

Fig. 5: Total number of CALB2+ type II hair cells are unaltered in the utricular extrastriola of Otof-/- *mice.* A-C. High-power confocal micrographs revealed several CALB2+ (green) type II hair cells (arrowheads) within the extrastriolae of *WT* (A), *Otof*+/- (B), and *Otof-/-* (C) mice (scale bar = 25 µm). TUBB3 (grayscale) in each specimen was used to delineate type I hair cells and aided in establishing a threshold for CALB2 (arrows). D. Bootstrap resampling statistics confirming that the total number of CALB2+ type II hair cells can be obtained by randomly resampling CALB2+/CALB2- hair cells from a virtual bin containing data from all three genotypes. The histogram (blue) represents the distribution of resampled *F*-statistics (genotype) obtained from 10,000 two-way ANOVAs ran using the resampled data. The red inverted triangle represents the *F*-statistic obtained from a similar two-way ANOVA executed with the empirical data ($F = 0.195$), which has been superimposed over the resampled data. The probability of

obtaining such an *F*-statistic by randomly resampling from all genotypes is p=0.589, suggesting that the observed CALB2+ hair cell counts are similar between the three genotypes.

TABLES

Table 1

Target	Manufacturer (Product #)	Immunogen	Host	Working Conc.	Positive Control	Negative Control
Primary Antibodies						
CALB1	Millipore-Sigma (C9848)	Bovine kidney calbindin-D	Mouse	1:125	-	Primary Ab omission
CALB2	Millipore-Sigma (MAB1568)	Recombinant rat calretinin	Mouse	1:125	-	Primary Ab omission
OCM	Santa Cruz (sc-7446)	Peptide mapping N-terminus of h-OCM	Goat	1:250	Hoffman et al. 2018	Primary Ab omission
TUBB3	BioLegend (Poly18020)	Rat brain microtubules	Rabbit	1:250	-	Primary Ab omission
OTOF	Abcam (ab53233)	Tagged fusion protein, corresponding to amino acids 1-395 of Human Otoferlin	Mouse	1:250	-	Primary Ab omission
Secondary Antibodies						
Anti-Mouse	Invitrogen (A21202)	Gamma Immunoglobulin Heavy and Light chains	Donkey	1:250	-	-
Anti-Goat	Invitrogen (A21432)	Gamma Immunoglobulin Heavy and Light chains	Donkey	1:250	-	-
Anti-TUBB3	Invitrogen (A31573)	Gamma Immunoglobulin Heavy and Light chains	Donkey	1:250	-	-

REFERENCES

Beurg M, Safieddine S, Roux I, Bouleau Y, Petit C, Dulon D (2008) Calcium- and otoferlin-dependent exocytosis by immature outer hair cells. J Neurosci 28:1798-1803.

Beurg M, Michalski N, Safieddine S, Bouleau Y, Schneggenburger R, Chapman ER, Petit C, Dulon D (2010) Control of exocytosis by synaptotagmins and otoferlin in auditory hair cells. J Neurosci 30:13281-13290.

Bonsacquet J, Brugeaud A, Compan V, Desmadryl G, Chabbert C (2006) AMPA type glutamate receptor mediates neurotransmission at turtle vestibular calyx synapse. J Physiol 576:63-71.

Cummings DM, Henning HE, Brunjes PC (1997) Olfactory bulb recovery after early sensory deprivation. J Neurosci 17:7433-7440.

Dechesne CJ, Rabejac D, Desmadryl G (1994) Development of calretinin immunoreactivity in the mouse inner ear. J Comp Neurol 346:517-529.

Dememes D, Lleixa A, Dechesne CJ (1995) Cellular and subcellular localization of AMPA-selective glutamate receptors in the mammalian peripheral vestibular system. Brain Res 671:83-94.

Desai SS, Zeh C, Lysakowski A (2005a) Comparative morphology of rodent vestibular periphery. I. Saccular and utricular maculae. J Neurophysiol 93:251-266.

Desai SS, Ali H, Lysakowski A (2005b) Comparative morphology of rodent vestibular periphery. II. Cristae ampullares. J Neurophysiol 93:267-280.

Dulon D, Safieddine S, Jones SM, Petit C (2009) Otoferlin is critical for a highly sensitive and linear calcium-dependent exocytosis at vestibular hair cell ribbon synapses. J Neurosci 29:10474-10487.

Hackney CM, Mahendrasingam S, Penn A, Fettiplace R (2005) The concentrations of calcium buffering proteins in mammalian cochlear hair cells. J Neurosci 25:7867-7875.

Hoffman LF, Choy KR, Sultemeier DR, Simmons DD (2018) Oncomodulin Expression Reveals New Insights into the Cellular Organization of the Murine Utricle Striola. J Assoc Res Otolaryngol 19:33-51.

Kevetter GA, Leonard RB (2002) Decreased expression of calretinin and calbindin in the labyrinth of old gerbils. Brain Res 957:362-365.

Li A, Xue J, Peterson EH (2008) Architecture of the mouse utricle: macular organization and hair bundle heights. J Neurophysiol 99:718-733.

Liberman MC, Liberman LD, Maison SF (2015) Chronic Conductive Hearing Loss Leads to Cochlear Degeneration. PLoS One 10:e0142341.

Martini M, Rossi ML, Rubbini G, Rispoli G (2000) Calcium currents in hair cells isolated from semicircular canals of the frog. Biophys J 78:1240-1254.

Moser T, Brandt A, Lysakowski A (2006) Hair cell ribbon synapses. Cell Tissue Res 326:347-359.

Mwachaka PM, Saidi H, Odula PO, Mandela PI (2015) Effect of Monocular Deprivation on Rabbit Neural Retinal Cell Densities. J Ophthalmic Vis Res 10:144-150.

Plotnik M, Marlinski V, Goldberg JM (2002) Reflections of efferent activity in rotational responses of chinchilla vestibular afferents. J Neurophysiol 88:1234-1244.

Prins TJ, Saldate JJ, Berke GS, Hoffman LF (2019) On the Legacy of Genetically Altered Mouse Models to Explore Vestibular Function: Distribution of Vestibular Hair Cell Phenotypes in the Otoferlin-Null Mouse. Ann Otol Rhinol Laryngol 128:125S-133S.

Puyal J, Sage C, Dememes D, Dechesne CJ (2002) Distribution of alpha-amino-3-hydroxy-5-methyl-4 isoazolepropionic acid and N-methyl-D-aspartate receptor subunits in the vestibular and spiral ganglia of the mouse during early development. Brain Res Dev Brain Res 139:51-57.

Qi Y, Yu S, Du Z, Qu T, He L, Xiong W, Wei W, Liu K, Gong S (2019) Long-Term Conductive Auditory Deprivation During Early Development Causes Irreversible Hearing Impairment and Cochlear Synaptic Disruption. Neuroscience 406:345-355.

Ramakrishnan NA, Drescher MJ, Morley BJ, Kelley PM, Drescher DG (2014) Calcium regulates molecular interactions of otoferlin with soluble NSF attachment protein receptor (SNARE) proteins required for hair cell exocytosis. J Biol Chem 289:8750-8766.

Ross MD (1994) A spaceflight study of synaptic plasticity in adult rat vestibular maculas. Acta Otolaryngol Suppl 516:1-14.

Roux I, Safieddine S, Nouvian R, Grati M, Simmler MC, Bahloul A, Perfettini I, Le Gall M, Rostaing P, Hamard G, Triller A, Avan P, Moser T, Petit C (2006) Otoferlin, defective in a human deafness form, is essential for exocytosis at the auditory ribbon synapse. Cell 127:277-289.

Safieddine S, Wenthold RJ (1999) SNARE complex at the ribbon synapses of cochlear hair cells: analysis of synaptic vesicle- and synaptic membrane-associated proteins. Eur J Neurosci 11:803-812.

Schiffmann SN, Cheron G, Lohof A, d'Alcantara P, Meyer M, Parmentier M, Schurmans S (1999) Impaired motor coordination and Purkinje cell excitability in mice lacking calretinin. Proc Natl Acad Sci U S A 96:5257-5262.

Simmons DD, Tong B, Schrader AD, Hornak AJ (2010) Oncomodulin identifies different hair cell types in the mammalian inner ear. J Comp Neurol 518:3785-3802.

Su ZL, Jiang SC, Gu R, Yang WP (1995) Two types of calcium channels in bullfrog saccular hair cells. Hear Res 87:62-68.

Sudhof TC (2004) The synaptic vesicle cycle. Annu Rev Neurosci 27:509-547.

Sultemeier DR, Choy KR, Schweizer FE, Hoffman LF (2017) Spaceflight-induced synaptic modifications within hair cells of the mammalian utricle. J Neurophysiol 117:2163-2178.

Tong B, Hornak AJ, Maison SF, Ohlemiller KK, Liberman MC, Simmons DD (2016) Oncomodulin, an EF-Hand Ca2+ Buffer, Is Critical for Maintaining Cochlear Function in Mice. J Neurosci 36:1631-1635.

Vincent PF, Bouleau Y, Safieddine S, Petit C, Dulon D (2014) Exocytotic machineries of vestibular type I and cochlear ribbon synapses display similar intrinsic otoferlin-dependent Ca2+ sensitivity but a different coupling to Ca2+ channels. J Neurosci 34:10853-10869.